

Superconducting gap structure of $\text{BaFe}_2(\text{As}_{1-x}\text{P}_x)_2$

L. Malone,¹ Y. Mizukami,^{2,3} P. Walmsley,¹ C. Putzke,¹ S. Kasahara,² T. Shibauchi,^{2,3} Y. Matsuda,² and A. Carrington¹

¹*H. H. Wills Physics Laboratory, University of Bristol, Tyndall Avenue, Bristol, BS8 1TL, United Kingdom.*

²*Department of Physics, Kyoto University, Sakyo-ku, Kyoto 606-8502, Japan.*

³*Department of Advanced Materials Science, University of Tokyo, Kashiwa, Chiba 277-8561, Japan*

We present a study of the superconducting gap structure in the iron-pnictide series $\text{BaFe}_2(\text{As}_{1-x}\text{P}_x)_2$. By measuring the variation of the specific heat as a function of temperature and magnetic field we are able to determine the number and Fermi surface location of the nodes in the superconducting gap. In particular, from measurements of the variation of the specific heat as the magnetic field is rotated in the ab plane of the sample we conclude that the nodes are in the $[110]$ directions. Then from a quantitative analysis of the temperature and field dependence of the specific heat we further conclude that nodes exist on all Fermi surface sheets.

Amongst the different families of unconventional superconductors, the iron-pnictides seem to be unique in that the structure of the superconducting energy gap Δ , i.e., how it varies with momentum \mathbf{k} on each Fermi surface sheet, can vary dramatically between different materials [1, 2]. This is despite the fact that the Fermi surfaces of all the iron-pnictides are quite similar, consisting of quasi-two-dimensional electron and hole pockets [3, 4]. It has been proposed theoretically that subtle differences in the Fermi surface topology, and possible structure of the magnetic interactions, can lead to a switch between different gap structures [5–7]. Also it has been proposed that certain gap structure can only be explained by orbital fluctuations perhaps in combination with spin fluctuations [8, 9]. The structure of Δ and how this varies between different iron-pnictide compounds therefore provides a strong test to discriminate between candidate microscopic theories of the superconductivity [2].

The materials which provide the best discrimination are those which have the most structure in $\Delta(\mathbf{k})$. In this sense, $\text{BaFe}_2(\text{As}_{1-x}\text{P}_x)_2$ is perhaps the most important example because it has a nodal gap structure [10] and also a high T_c , reaching a maximum value of 30 K at $x = 0.30$. In most other iron-pnictides $\Delta(\mathbf{k})$ does not exhibit nodes [2] although in some systems the experimental evidence is somewhat ambiguous because of strong impurity scattering. LaFePO [11], LiFeP [12] are exceptions which do show evidence for nodes but both of these have a low T_c (< 7 K). $\text{BaFe}_2(\text{As}_{1-x}\text{P}_x)_2$ also has the advantage that in high quality single crystals, the electron mean free path is very high, as evidenced by the observation of de Haas-van Alphen oscillations [13, 14], and so the gap structure is not strongly smeared by impurity scattering.

Although bulk probes including magnetic penetration depth λ [10], nuclear magnetic resonance [15] and thermal conductivity [10, 16] have shown that $\text{BaFe}_2(\text{As}_{1-x}\text{P}_x)_2$ has a nodal gap structure, the position, number, and orientation of these nodes is still unclear. Although angle resolved photoemission spectroscopy (ARPES) can in principle resolve this issue results to date have been

inconsistent [8, 9, 17]. Here we show from a study of the temperature and magnetic field-angle dependence of the specific heat that $\text{BaFe}_2(\text{As}_{1-x}\text{P}_x)_2$ has *vertical* line nodes in the $[110]$ directions and that nodes exist on both the electron and the hole sheets.

Single crystals of $\text{BaFe}_2(\text{As}_{1-x}\text{P}_x)_2$ were grown using a self-flux method [18] and the phosphorous content x was measured using energy dispersive x-ray analysis (EDX) with an accuracy of ± 0.02 in x . The specific heat was measured using a custom built calorimeter [19, 20] run in two modes: a relaxation mode to measure the temperature dependence at fixed field and an AC mode to measure the field angle dependence at fixed temperature. After each rotation of the field, the sample was heated above T_c and field cooled to minimize any effects of flux pinning. Our technique allowed us to measure small single crystals; the samples measured here had masses between 50 and 300 μg . The absolute calibration of the calorimeter was checked with a high purity Ag sample and deviations from standard data were below 1% in fields up to 14 T.

We begin by discussing the temperature dependence of the specific heat of a sample of $\text{BaFe}_2(\text{As}_{1-x}\text{P}_x)_2$ with $x = 0.47$. This particular composition was selected because H_{c2} can be exceeded easily with the available magnetic field. Fig. 1(a) shows the specific heat of this sample measured in 0 T and 10 T. A superconducting transition is observed at 17.5 K in 0 T which is completely suppressed with a field of 10 T. To obtain the electronic contribution to the heat capacity, the 10 T data is assumed to consist of a field independent phonon term plus a linear electronic term $\gamma_n T$. The phonon contribution is then subtracted from the 0 T data to obtain the electronic contribution to the specific heat C_e in the superconducting state (Fig. 1(b)). We have verified that $\int_0^{T_c} C_e/T dT$ is equal to $\gamma_n T_c$ at T_c within experimental error confirming that the C_e has been accurately isolated. We find that C_e/T varies linearly with T at low temperature and is well fitted by a nodal gap model (described in more detail later), confirming the presence of

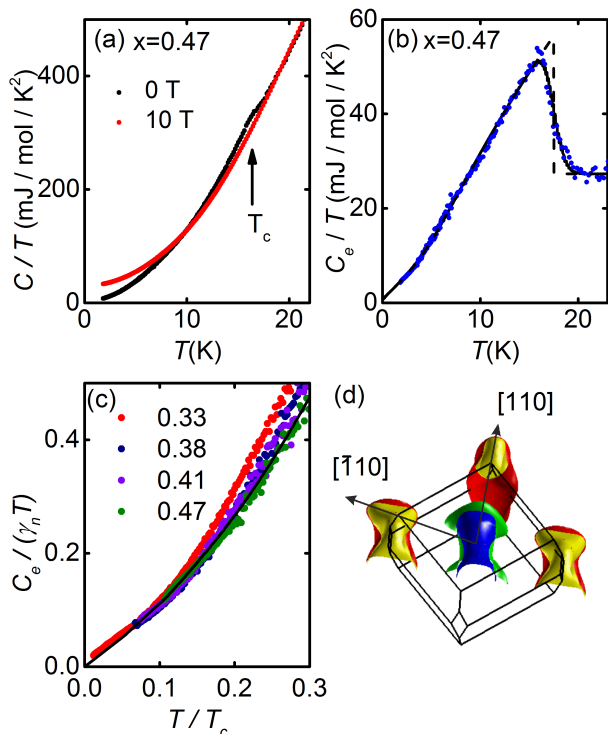


FIG. 1: (color online). (a) Specific heat versus temperature in 0 T and 10 T ($H||c$) for $\text{BaFe}_2(\text{As}_{1-x}\text{P}_x)_2$ with $x = 0.47$ ($T_c = 17.5$ K). (b) Electronic heat capacity in the superconducting state. The solid line is a fit to a nodal structure as described in the text convoluted with a Gaussian spread of transition temperatures $\delta T_c/T_c = 0.03$. The dashed line is the fit without the convolution. (c) Specific heat versus temperature divided by γT_c for several values of x . The line is fit to $x = 0.47$ data as shown in (b). (d) Schematic of the Fermi surface showing the electron and hole sheets at the zone corner and center respectively.

gap nodes at this composition. For higher T_c samples our available magnetic field (≤ 14 T) is insufficient to completely suppress superconductivity, however, by assuming that the phonon term does not change appreciably with x we can estimate C_e for all x . In Fig. 1(c) we show the low temperature specific heat for several different values of x with the same $x = 0.47$ phonon term subtracted. The data are shown on normalized axes ($C_e/\gamma_n T$ versus T/T_c), where γ_n was determined from the height of the superconducting anomaly as in Ref. [14]. It can be seen that they all tend towards the same limiting behavior as $T/T_c \rightarrow 0$ where differences in phonon terms become negligible. This is consistent with Ref. [21] where it was found that the size of the linear term in $\lambda(T)/\lambda(T=0)$ was also independent of x . As the size of linear terms in both $C_e/(\gamma_n T)$ and $\lambda(T)/\lambda(T=0)$ depend on the number and structure of the gap nodes, these results indicate that the gap structure does not change appreciably with x in $\text{BaFe}_2(\text{As}_{1-x}\text{P}_x)_2$.

We now turn to the question of the direction of the

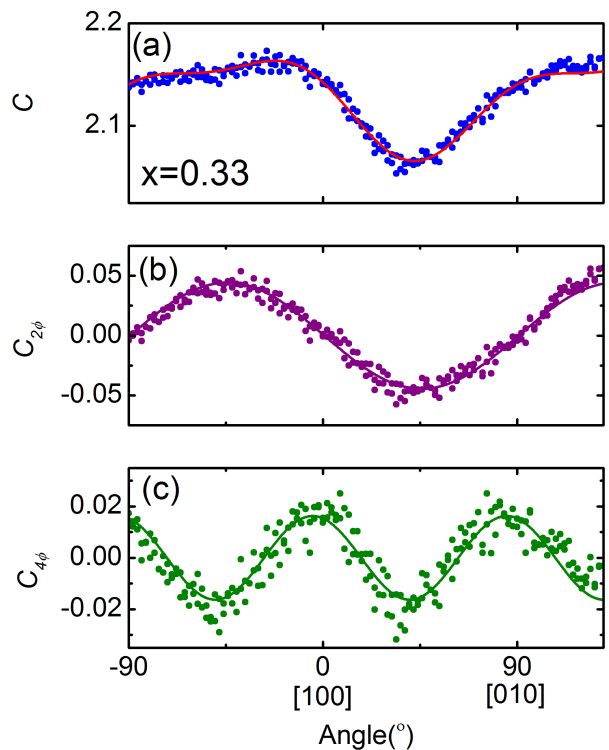


FIG. 2: (color online). (a) Specific heat of $\text{BaFe}_2(\text{As}_{1-x}\text{P}_x)_2$ ($x = 0.33$, $T_c = 28.8$ K) as a function of angle as the field is rotated between the a and b axis. The line is a fit to Eq. 1. (b) and (c) show the same data with the fitted $C_{4\phi}$ and $C_{2\phi}$ terms respectively plus the constant C_0 subtracted. The units of C in all panels are $\text{mJ mol}^{-1}\text{K}^{-1}$.

nodes in the superconducting gap. For this study a sample close to optimal composition ($x = 0.33$, $T_c = 28.8$ K) was selected so that we can more easily reach the low T/T_c and H/H_{c2} limits. Fig. 2 shows the specific heat as a function of field angle at a fixed temperature as the field is rotated between the a and b axis. The data are well fitted by a constant and two terms which have two fold and four fold symmetry

$$C(\phi) = C_0 + C_{2\phi} + C_{4\phi} \quad (1)$$

Here ϕ is the in-plane angle measured relative to the a -axis ([100] direction) and $C_{n\phi} = c_n \cos(n\phi + \delta_n)$. At $T = 0.5$ K and $\mu_0 H = 3$ T (Fig. 2) the twofold component ($C_{2\phi}$) has a peak to peak amplitude of $\sim 5\%$ of the total C , and the fourfold term $c_4 \simeq 0.5c_2$. The phases $\delta_2 = 89 \pm 1^\circ$ and $\delta_4 = 19 \pm 2^\circ$, correspond to the c_2 being zero at $+1^\circ$ and c_4 being maximum at -5° off the a -axis. The sample alignment with the field axis is accurate to $\pm 3^\circ$ so within error both c_2 and c_4 are approximately aligned with the crystal axes.

Theory suggests that there are two mechanisms which can give rise to a field-angle dependence of C . First there is a contribution from the anisotropy of the Fermi velocity v_F and a second from the structure of Δ . The for-

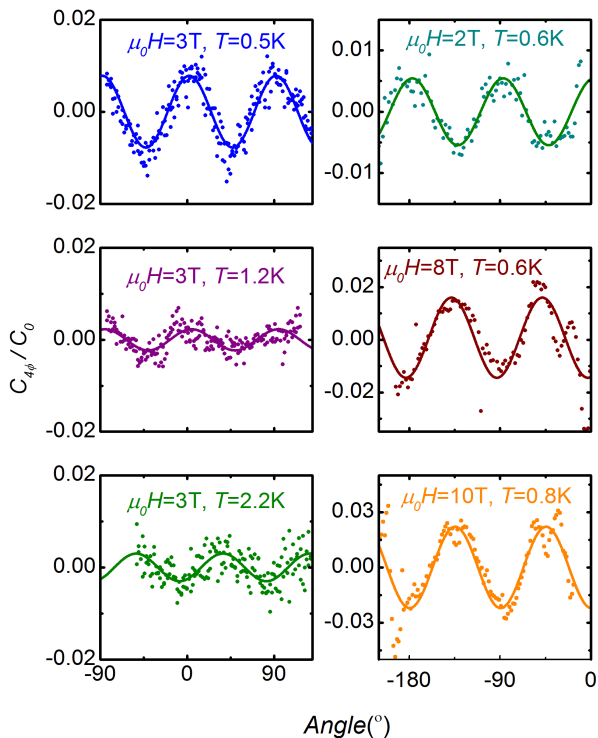


FIG. 3: (color online). Fourfold component of the same sample as in Fig. 2 at several fields and temperatures.

mer is expected to have a weak dependence on T and H whereas the latter has a much stronger dependence. We find that for $\text{BaFe}_2(\text{As}_{1-x}\text{P}_x)_2$ the twofold component does not depend strongly on T or H [22] and therefore likely arises from an anisotropy in v_F , similar to the two fold field angular dependence of the normal state magnetic torque [23]. In Fig. 3 we show the oscillation data at several different values of T and B with the two fold term subtracted. We see that the fourfold term varies strongly as a function of T and H and is therefore likely to originate from the gap anisotropy. Theory suggests that for a nodal superconductor in the low T and B limit there is a minima in C whenever the field is applied parallel to a node [24, 25]. This effect has been observed in several nodal superconductors [20, 26]. So as c_4 is minimum when H is aligned approximately along the [110] directions, we conclude that there are quasi-two-dimensional vertical line nodes located along these directions. This result is consistent with angle dependent thermal conductivity measurements [16] which showed a four fold term with minima in the same directions as C and also a similarly strong twofold component.

Theoretical studies [24, 27] have shown that as the temperature is raised from zero and the quasiparticle states near the nodes are thermally occupied, the size of the nodal contribution c_4 decreases and eventually crosses zero and becomes inverted, so there is then a maximum in C when H is parallel to a node. Also, as the field

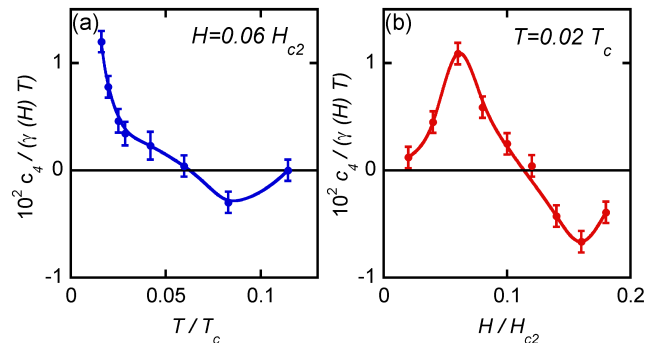


FIG. 4: (Color Online) Amplitude of the fourfold component of the the specific heat c_4 , of the same sample as in Fig. 2 as a function of (a) temperature and (b) field. $T_c = 28.8$ K and $\mu_0 H_{c2} = 50$ T. Lines are guides to the eye.

increases from zero at low T , c_4 is expected to increase, reach a maximum then again cross zero producing a negative c_4 . In Fig. 4 we show the T and H dependence of c_4 in our sample which displays both of these effects. c_4 decreases sharply as a function of temperature, crosses zero at $T/T_c \simeq 0.05$, and shows a inversion at $T/T_c \simeq 0.08$. Following the trend to high temperature becomes significantly more difficult because of the strongly increasing phonon background. The field dependence of c_4 displays a maximum at around 3 T which is $H/H_{c2} \simeq 0.05$, and then crosses zero at $H/H_{c2} \simeq 0.11$ and becomes inverted and again reaches a negative maximum at $H/H_{c2} \simeq 0.16$. This behavior is very similar to that observed in the d -wave heavy fermion superconductor CeCoIn_5 where the change in sign of c_4 occurs at almost the same reduced field as here [28].

Although the angle dependent measurements unambiguously identify the direction of the line-nodes, these measurements are less clear regarding on which Fermi surface sheet(s) the nodes are located. In principle, such information might be extracted from the amplitude of the oscillations and the details of the T and H dependence, although this would require extensive modelling and may not be robust to the necessary simplifying assumptions of the theoretical model. So in order to answer this important remaining question we analyze in more detail the temperature and field dependence of C at fixed angle $H \parallel c$. For this we use the data for the $x = 0.47$ sample where we are most confident of the phonon background subtraction.

We begin by fitting the temperature dependent data to a simple model, where the gap has a fourfold line node structure on both the electron (e) and hole (h) sheets,

$$\Delta_{e,h} = \Delta_0 \cos(2\phi). \quad (2)$$

As shown in Fig. 1b, this model [19, 22] provides an excellent fit of the data with the single fitting parameter $\Delta_0 = 2.1 \pm 0.1 k_B T_c$ ($\gamma_n = 27.7$ mJ/mol/K² is fixed by the

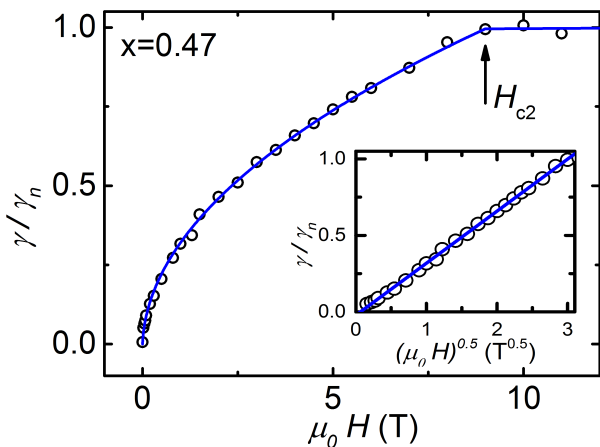


FIG. 5: (color online). Field dependence of the Sommerfeld coefficient γ of $\text{BaFe}_2(\text{As}_{1-x}\text{P}_x)_2$ with $x = 0.47$. The line shows a fit a fit to $\gamma(H) = AH^{\frac{1}{2}}$ below H_{c2} and a constant above this. Inset: The same data plotted versus $H^{\frac{1}{2}}$.

normal state value). This gap structure and value of Δ_0 is consistent with $\lambda(T)$ data for the same system. Within the same gap model, at low temperature $\Delta\lambda(T)/\lambda(0) = (\ln(2)k_B T)/\Delta_0$, giving $(T_c d\lambda/dT)/\lambda(0) \simeq 0.33$ which is close to the experimental, approximately x independent value of 0.4 ± 0.1 [21]. This value of Δ_0 is close to that expected from the single band d -wave model in the weak-coupling limit $\Delta_0 = 2.1k_B T_c$ [29] although our measurements are not sensitive to the phase of the Δ so we can not distinguish between A_{1g} and B_{1g} gap symmetry. The disorder dependence of $\lambda(T)$ suggests that the symmetry is A_{1g} [30].

Although, this form of the gap function provides an excellent description of the data with a single parameter, the fit alone cannot exclude more complicated multigap forms. Gap functions where there are line or loop nodes on either the hole or electron sheets but not on both have been proposed [16, 31, 32]. In general, line nodes will always give a T^2 contribution to C for $T \ll T_c$ the coefficient of which (α) will depend on the number of nodes, the gap slope $\eta = d\Delta/d\phi$ and v_F at the node. So reducing the number of nodes (for example having them on the electron sheets only) will reduce α but this can be compensated for by reducing η . The jump at T_c ($\Delta C/(\gamma_n T_c)$) on the other hand, will depend on the Fermi surface averaged value of $(d\Delta^2/dT)/v_F$. So in general, the essential parameters of any possible gap function, with respect to fitting the whole temperature dependence of the specific heat, are the number of nodes divided by the gap slope η and the average value of the gap over the whole Fermi surface. Clearly, there are many possible solutions which would also provide a reasonable fit to the data in Fig. 1(b) (see Ref. [22] for further details). However, all of these have considerably more structure in $\Delta(\mathbf{k})$ than Eq. 2.

To distinguish further between these single or multigap scenarios we turn to the field dependence of the specific heat. In a nodal superconductor, in the clean limit, at $T = 0$ and $0 < H \ll H_{c2}$ we should expect that $C_e \sim \gamma T$, with $\gamma \sim H^{\frac{1}{2}}$. This was first observed in the cuprate superconductor $\text{YBa}_2\text{Cu}_3\text{O}_{7-\delta}$ [33] but has now been seen in many different materials. At higher H we might expect some departure from this simple form but nevertheless we would expect $\gamma(H)$ to evolve smoothly. On the other hand, in the multigap case, we would expect significant structure in $\gamma(H)$. For example, if there is a much smaller gap on one sheet relative to another we would expect γ to increase strongly below a field scale set by the small gap and then more slowly thereafter. This behavior has been experimentally observed in both fully gapped and nodal multigap superconductors such as MgB_2 [34], KFe_2As_2 [35] and Sr_2RuO_4 [36]. Also, if there was a large constant gap on one sheet and a nodal gap on the another, we would expect at low fields a $H^{\frac{1}{2}}$ contribution from the nodal part and a much smaller linear H contribution from the fully gapped part [37]. In this case, as H approaches H_{c2} , $\gamma(H)$ would necessarily have to rise rapidly towards γ_n . So the form of $\gamma(H)$ is a further constraint on possible gap structures.

To extract $\gamma(H)$ for our sample of $\text{BaFe}_2(\text{As}_{1-x}\text{P}_x)_2$ ($x=0.47$) we measure the T dependence at several fixed fields and fit C/T to a second order polynomial with the phonon term fixed to the high field value. As shown in Fig. 5 we find that $\gamma(H)$ is well described by the nodal model; $\gamma(H) = \beta\gamma_n(H/H_{c2})^{\frac{1}{2}}$ from low field all the way up to H_{c2} , with $\beta = 1.05 \pm 0.02$ very close to unity. There is no additional structure in $\gamma(H)$, such as upturns close to H_{c2} , plateaus or other features. This strongly indicates that there are no fully gapped sheets of Fermi surface. It suggests that the gap structure is simple and evolves smoothly with field. We find very similar behavior of $\gamma(H)$ for $x = 0.41$ [22].

Although our data are most simply explained by the above single nodal gap model, we cannot rule out the possibility of there being horizontal rather than vertical nodes on some of the Fermi surface sheets. Also, loop nodes, provided that the ϕ separation of the loop is small, so they approximate a single line node and therefore do not generate higher harmonics in $C(H, \phi)$, may also be consistent with our data. More detailed theoretical modelling of $C(T, H, \phi)$ with realistic Fermi surface parameters would help to resolve this. The direction of the nodes is consistent with the gap anisotropy observed by ARPES measurements [9] on one of the electron sheets, however the lack of observation of nodes on the hole sheets in the same study (and Ref. [8]) is inconsistent with our $\gamma(H)$ results. The results might be reconciled if the nodal hole sheet gap is more sensitive to disorder or different at the sample surface. Indeed horizontal nodes on one of the hole sheets were reported by a different ARPES study [17].

In summary, our measurement of the specific heat of $\text{BaFe}_2(\text{As}_{1-x}\text{P}_x)_2$ show that gap nodes exist along the [110] (Fe-Fe bond) direction. The data further suggest that nodes exist on all the Fermi surface sheets. The quantitative agreement of the low temperature specific heat and magnetic penetration depth for values of x across the superconducting part of the phase diagram suggest that this gap function does not vary significantly with x .

We thank P. Hirschfeld and I. Vekhter for useful discussions. This work was supported by the Engineering and Physical Sciences Research Council (Grant No. EP/H025855/1) and Topological Quantum Phenomena” (No. 25103713) Grant-in Aid for Scientific Research on Innovative Areas from MEXT, and KAKENHI from JSPS.

-
- [1] A. Carrington, *Comptes Rendus Physique* **12**, 502 (2011).
 [2] P. J. Hirschfeld, M. M. Korshunov, and I. I. Mazin, *Rep. Prog. Phys.* **74**, 124508 (2011).
 [3] A. Carrington, *Reports on Progress in Physics* **74** (2011).
 [4] A. A. Kordyuk, *Low Temperature Physics* **38**, 888 (2012).
 [5] K. Kuroki, H. Usui, S. Onari, R. Arita, and H. Aoki, *Phys. Rev. B* **79**, 224511 (2009).
 [6] S. Graser, T. A. Maier, P. J. Hirschfeld, and D. J. Scalapino, *New J. Phys.* **11**, 025016 (2009).
 [7] R. Thomale, C. Platt, W. Hanke, and B. A. Bernevig, *Phys. Rev. Lett.* **106**, 187003 (2011).
 [8] T. Shimojima, F. Sakaguchi, K. Ishizaka, Y. Ishida, T. Kiss, M. Okawa, T. Togashi, C.-T. Chen, S. Watanabe, M. Arita, et al., *Science* **332**, 564 (2011).
 [9] T. Yoshida, S. Ideta, T. Shimojima, W. Malaeb, K. Shinada, H. Suzuki, I. Nishi, A. Fujimori, K. Ishizaka, S. Shin, et al., arXiv:1301.4818.
 [10] K. Hashimoto, M. Yamashita, S. Kasahara, Y. Senshu, N. Nakata, S. Tonegawa, K. Ikeda, A. Serafin, A. Carrington, T. Terashima, et al., *Phys. Rev. B* **81**, 220501 (2010).
 [11] J. D. Fletcher, A. Serafin, L. Malone, J. G. Analytis, J.-H. Chu, A. S. Erickson, I. R. Fisher, and A. Carrington, *Phys. Rev. Lett.* **102**, 147001 (2009).
 [12] K. Hashimoto, S. Kasahara, R. Katsumata, Y. Mizukami, M. Yamashita, H. Ikeda, T. Terashima, A. Carrington, Y. Matsuda, and T. Shibauchi, *Phys. Rev. Lett.* **108**, 047003 (2012).
 [13] H. Shishido, A. F. Bangura, A. I. Coldea, S. Tonegawa, K. Hashimoto, S. Kasahara, P. M. C. Rourke, H. Ikeda, T. Terashima, R. Settai, et al., *Phys. Rev. Lett.* **104**, 057008 (2010).
 [14] P. Walmsley, C. Putzke, L. Malone, I. Guillamon, D. Vignolles, C. Proust, S. Badoux, A. I. Coldea, M. D. Watson, S. Kasahara, et al., *Phys. Rev. Lett.* **110**, 257002 (2013).
 [15] Y. Nakai, T. Iye, S. Kitagawa, K. Ishida, S. Kasahara, T. Shibauchi, Y. Matsuda, and T. Terashima, *Phys. Rev. B* **81**, 020503 (2010).
 [16] M. Yamashita, Y. Senshu, T. Shibauchi, S. Kasahara, K. Hashimoto, D. Watanabe, H. Ikeda, T. Terashima, I. Vekhter, A. B. Vorontsov, et al., *Phys. Rev. B* **84**, 060507 (2011).
 [17] Y. Zhang, Z. R. Ye, Q. Q. Ge, F. Chen, J. Jiang, M. Xu, B. P. Xie, and D. L. Feng, *Nat. Phys.* **8**, 371 (2012).
 [18] S. Kasahara, T. Shibauchi, K. Hashimoto, K. Ikeda, S. Tonegawa, R. Okazaki, H. Shishido, H. Ikeda, H. Takeya, K. Hirata, et al., *Phys. Rev. B* **81**, 184519 (2010).
 [19] O. Taylor, A. Carrington, and J. Schlueter, *Phys. Rev. Lett.* **99**, 057001 (2007).
 [20] L. Malone, O. Taylor, J. Schlueter, and A. Carrington, *Phys. Rev. B* **82**, 014522 (2010).
 [21] K. Hashimoto, K. Cho, T. Shibauchi, S. Kasahara, Y. Mizukami, R. Katsumata, Y. Tsuruhara, T. Terashima, H. Ikeda, M. A. Tanatar, et al., *Science* **336**, 1554 (2012).
 [22] See supplementary material at <http://link.aps.org/supplemental/xxx> for additional details.
 [23] S. Kasahara, H. J. Shi, K. Hashimoto, S. Tonegawa, Y. Mizukami, T. Shibauchi, K. Sugimoto, T. Fukuda, T. Terashima, A. H. Nevidomskyy, et al., *Nature* **486**, 382 (2012).
 [24] I. Vekhter, P. Hirschfeld, J. Carbotte, and E. Nicol, *Phys. Rev. B* **59**, R9023 (1999).
 [25] A. Vorontsov and I. Vekhter, *Phys. Rev. Lett.* **105**, 187004 (2010).
 [26] H. Aoki, T. Sakakibara, H. Shishido, R. Settai, Y. Onuki, P. Miranovic, and K. Machida, *J. Phys. Cond. Mat.* **16**, L13 (2004).
 [27] A. Vorontsov and I. Vekhter, *Phys. Rev. Lett.* **96**, 237001 (2006).
 [28] K. An, T. Sakakibara, R. Settai, Y. Onuki, M. Hiragi, M. Ichioka, and K. Machida, *Phys. Rev. Lett.* **104**, 037002 (2010).
 [29] H. Won and K. Maki, *Phys. Rev. B* **49**, 1397 (1994).
 [30] Y. Mizukami, M. Konczykowski, Y. Kawamoto, S. Kurata, S. Kasahara, K. Hashimoto, V. Mishra, A. Kreisel, Y. Wang, P. J. Hirschfeld, et al., arXiv:1405.6951.
 [31] S. Graser, A. F. Kemper, T. A. Maier, H.-P. Cheng, P. J. Hirschfeld, and D. J. Scalapino, *Phys. Rev. B* **81**, 214503 (2010).
 [32] K. Suzuki, H. Usui, and K. Kuroki, *J. Phys. Soc. Jpn.* **80**, 013710 (2011).
 [33] K. A. Moler, D. J. Baar, J. S. Urbach, R. Liang, W. N. Hardy, and A. Kapitulnik, *Phys. Rev. Lett.* **73**, 2744 (1994).
 [34] F. Bouquet, Y. Wang, I. Sheikin, T. Plackowski, A. Junod, S. Lee, and S. Tajima, *Phys. Rev. Lett.* **89**, 257001 (2002).
 [35] F. Hardy, R. Eder, M. Jackson, D. Aoki, C. Paulsen, T. Wolf, P. Burger, A. Boehmer, P. Schweiss, P. Adelman, et al., arxiv p. 1309.5654 (2013).
 [36] K. Deguchi, Z. Mao, H. Yaguchi, and Y. Maeno, *Phys. Rev. Lett.* **92**, 047002 (2004).
 [37] Y. Wang, J. S. Kim, G. R. Stewart, P. J. Hirschfeld, S. Graser, S. Kasahara, T. Terashima, Y. Matsuda, T. Shibauchi, and I. Vekhter, *Phys. Rev. B* **84**, 184524 (2011).

Supplementary Information

Temperature and field dependence of twofold term

The temperature and field dependence of the amplitude of the twofold term c_2 extracted from the specific heat as a function of field angle is plotted in Figure S1. The variation of c_2 in the range measured is small relative to that of c_4 (see main text).

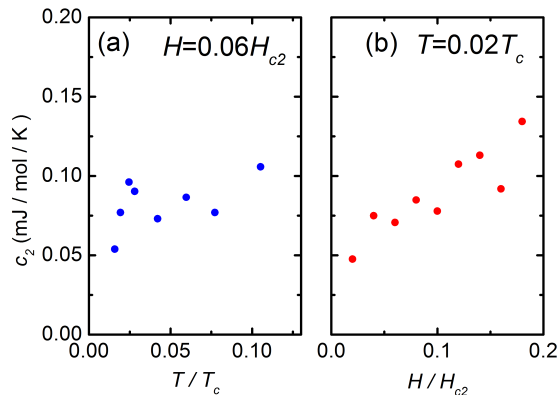


FIG. 6: Amplitude of the twofold component c_2 of the specific heat as a function of (a) temperature and (b) field.

Field dependence of γ

To extract the field dependence of γ , the specific heat versus temperature is measured in multiple fields, using a carefully field calibrated calorimeter. The data are fitted to the form $\frac{C}{T} = \gamma + AT + BT^2$, where the phonon term $B = 1.1$ mJ/mol/K⁴ is fixed independent of field. Figure S3 shows the data with the fits for several applied fields.

Figure S4 shows $\gamma(H)$ for the 0.47 and 0.41 samples. For the $x = 0.41$ sample, γ was extracted from the jump at T_c to be 38 mJ/mol/K² and H_{c2} was determined to be 30 T by comparison to samples with the same x and T_c [4]. The $\gamma(H)$ data are fitted to $\frac{\gamma}{\gamma_n} = \beta \left(\frac{H}{H_{c2}}\right)^{1/2}$, the fitted values of β are 1.14 ± 0.1 for $x=0.41$ where the error primarily arises from the uncertainty on H_{c2} in this sample and 1.05 ± 0.02 for $x = 0.47$. Within error the size of β in the two samples is equal.

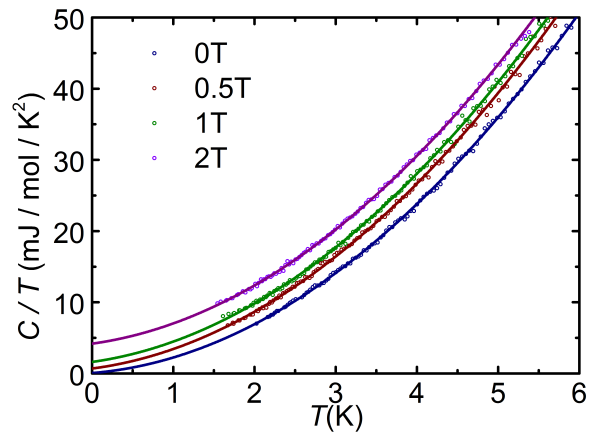


FIG. 7: Specific heat of $\text{BaFe}_2(\text{As}_{1-x}\text{P}_x)_2$ with $x = 0.47$ as a function of temperature in multiple fields. Lines are fits used to extract $\gamma(H)$.

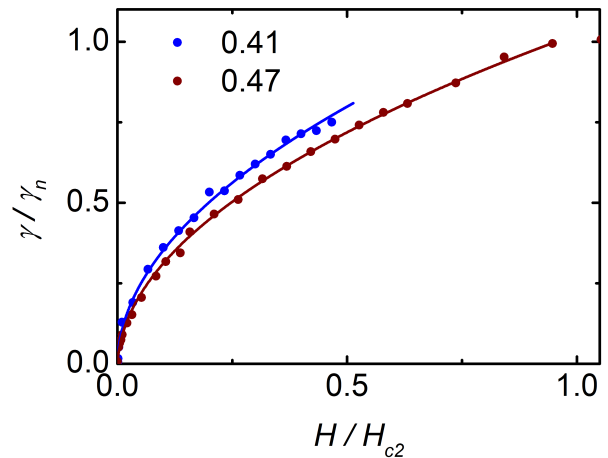


FIG. 8: Field dependence of $\gamma(H)$ for two samples of $\text{BaFe}_2(\text{As}_{1-x}\text{P}_x)_2$, $x = 0.41$ and $x = 0.47$.

Fitting temperature dependence of specific heat

We calculated the temperature dependence of the specific heat for a generalized superconducting energy gap function $\Delta_i = F_i(\phi, z)$ (where i represents each Fermi surface sheet and ϕ, z are cylindrical coordinates), using the following equation for the entropy

$$S_i = -\frac{k_B}{2\pi^3\hbar} \int_0^\infty \int \frac{1}{v_F(\mathbf{k})} ([1-f] \ln[1-f] + f \ln f) dS_f d\epsilon. \quad (3)$$

Here f is the fermi function $f = [\exp(E/(k_B T)) + 1]^{-1}$, E is the quasiparticle energy $E^2 = (\epsilon^2 + \Delta(\phi, z)^2)$, ϵ is the single particle energy, $v_F(\mathbf{k})$ is the normal state Fermi velocity and the integral dS_F is over each sheet of Fermi surface. The total heat capacity is then calculated using $C = T \sum \frac{\delta S_i}{\delta T}$. We found that for the gap structure considered here, the anisotropy of $v_F(\mathbf{k})$ (which we obtained from DFT band structure calculations) makes little difference to the specific heat fits and therefore we adopt a simpler form for the entropy where we approximate each Fermi sheet as a cylinder and weight the contribution of each sheet according to its relative contribution to the total density of states N . To obtain the relative weights of N we use the Fermi surface of BaFe_2P_2 , which gives : 20% (outer electron), 20% (inner electron), 23% (inner hole) and 37% (outer hole). It has been shown experimentally that the mass enhancements on each sheet are relatively uniform for all x [1, 2]. The total magnitude of N is set by γ_n which is experimentally determined above T_c . Finally, the fit is convoluted with a Gaussian spread of transition temperatures to describe the rounding near T_c . For the $x = 0.47$ sample this spread is found to be $\delta T_c/T_c = 0.03$.

In a nodal superconductor, the amplitude of the low temperature linear behavior is determined by the slope of the gap at the node $\eta = \frac{d\Delta}{d\phi}$ and the number of nodes. The simplest nodal function (Case (I)) has $F_{e,h} = \Delta_0 \cos(2\phi)$, and as the gap has the same structure on each sheet the relative weighting is redundant. This model fits the data very well over the entire temperature range as shown in Figure S2 and main text Figure 1. As discussed in the main text it is also possible to fit the data with a number of other different gap structures. To illustrate this point, Figures S2(b,c) show the data fitted to (Case (II)) a gap structure which has vertical nodes

on the electron sheets and an isotropic gap on the hole sheets, and (Case (III)) a loop node structure (as suggested in Ref. [3]) where the gap on the electron sheets follows, $F_e = \Delta_e(1 - |0.6 \cos(z)| - 0.6 \cos(z) \cos(2\phi))$ and the gap on the hole sheets is isotropic. The gap structures can be visualized in the insets to Figure S2. Comparing Case (I) to Case (II), it can be seen that in (II) the maximum gap on the electron sheets has decreased thus decreasing η and compensating for the lack of nodes on the hole sheets with respect to fitting the low temperature linear term in C/T . In addition, the isotropic gap on the hole sheet in (II) is increased relative to the average gap in (I), so that the size of the jump in C at T_c is reproduced. This illustrates the general principles outlined in the main text. For both (II) and (III) the fit is slightly worse than for model (I) even though there are more parameters, however, this alone is not sufficient to distinguish between the models. For example, the fit can be improved by allowing the exact form of the gap function in the loop node model to vary. However, as argued in the main text, the additional structure of the gaps in cases (II) and (III) compared to (I) would inevitable lead to additional structure in $\gamma(H)$ which was not observed. We therefore conclude that the thermodynamic data point to there being a simple nodal structure on all sheets. The structure does not have to be exactly the same as (I), for example we cannot rule out there being horizontal nodes on one of the sheets, but there must be nodes on all sheets to reproduce the observed $\gamma(H)$.

-
- [1] B. J. Arnold, S. Kasahara, A. I. Coldea, T. Terashima, Y. Matsuda, T. Shibauchi, and A. Carrington, Phys. Rev. B. **83**, 220504 (2011).
 - [2] P. Walmsley, C. Putzke, L. Malone, I. Guillamon, D. Vignolles, C. Proust, S. Badoux, A. I. Coldea, M. D. Watson, S. Kasahara, Y. Mizukami, T. Shibauchi, Y. Matsuda, and A. Carrington, Phys. Rev. Lett. **110**, 257002 (2013).
 - [3] M. Yamashita, Y. Senshu, T. Shibauchi, S. Kasahara, K. Hashimoto, D. Watanabe, H. Ikeda, T. Terashima, I. Vekhter, A. B. Vorontsov, and Y. Matsuda, Phys. Rev. B **84**, 060507 (2011).
 - [4] C. Putzke, P. Walmsley, J. Fletcher, L. Malone, D. Vignolles, C. Proust, S. Badoux, P. See, H. Beere, D. Ritchie, S. Kasahara, Y. Mizukami, T. Shibauchi, Y. Matsuda, and A. Carrington, arXiv:1402.1323.

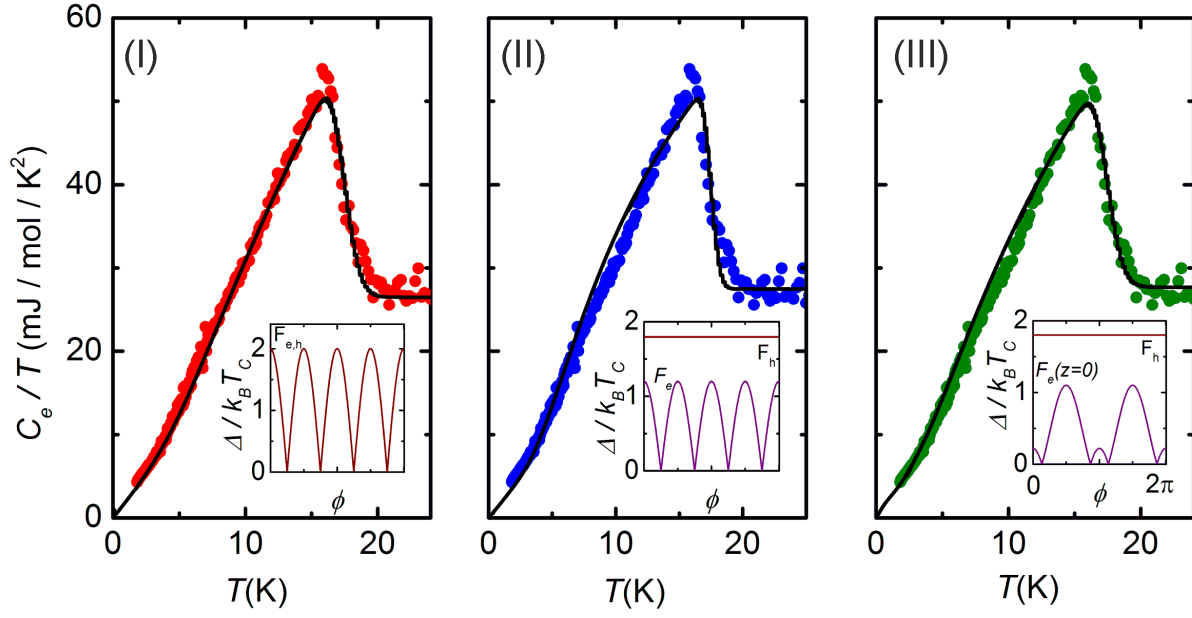


FIG. 9: Electronic specific in the superconducting state of $x = 0.47$ sample with three different fits. Case (I) nodes on all Fermi surface sheets. Case (II) vertical nodes on the electron sheets and isotropic gap on the hole sheets. Case (III) loop nodes on the electron sheets and isotropic gap on the hole sheets. The insets are the fitted gap structures on each sheet.